

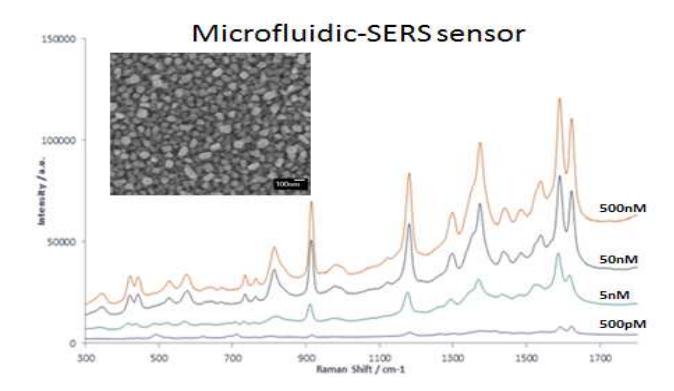
RSC Advances

In-situ Microfluidic Fabrication of SERS Nanostructures for Highly Sensitive Fingerprint Microfluidic-SERS Sensing

Journal:	RSC Advances
Manuscript ID:	RA-ART-11-2014-015174.R1
Article Type:	Paper
Date Submitted by the Author:	14-Jan-2015
Complete List of Authors:	Parisi, Joseph; University of Connecticut, Chemical, Materials and Biomolecular Engineering Department Dong, Qiuchen; University of Connecticut, Biomedical Engineering Lei, Yu; University of Connecticut, Chemical and Biomolecular Engineering Department

SCHOLARONE™ Manuscripts

ToC



A microfluidic-SERS device has been fabricated via a facile *in-situ* galvanic replacement for ultrasensitive detection of pesticide and herbicide.

Cite this: DOI: 10.1039/c0xx00000x

www.rsc.org/xxxxxx PAPER

In-situ Microfluidic Fabrication of SERS Nanostructures for Highly Sensitive Fingerprint Microfluidic-SERS Sensing

Joseph Parisi^a, Qiuchen Dong^b, and Yu Lei*^{ab}

Received (in XXX, XXX) Xth XXXXXXXXX 20XX, Accepted Xth XXXXXXXX 20XX 5 DOI: 10.1039/b000000x

A microfluidic device with integrated silver nanoparticles (AgNPs) was fabricated via *in-situ* galvanic replacement of pre-patterned copper substrate in a microfluidic channel. The integrated microfluidic device with AgNPs serves as a highly active Raman substrate which can be applied for in-channel surface-enhanced Raman scattering (SERS). Preparation of the SERS active substrate and subsequent SERS experiments are all completed within the microfluidic device allowing for easy integration and application. In conjunction with the high sensitivity, easy fabrication and mobility of the microfluidic device, the developed microfluidic-SERS system provides an excellent sensing platform for sensitive, real-time fingerprint detection of target molecules. Crystal violet is first used as a model compound to demonstrate the effectiveness of the microfluidic-SERS system. Specifically, the *in-situ* fabricated SERS active substrate demonstrates high sensitivity and exhibits an apparent enhancement factor of 2.2 × 10⁷, high robustness and reusability, making it a perfect fit for the real time detection of pesticides. Finally the detection of pesticide and herbicide such as Carbofuran and Alachlor as low as 5 ppb was demonstrated using the as-developed microfluidic-SERS system. This study opens a new avenue to fabricate an integrated microfluidic-SERS sensing system with high performance.

Introduction

Water pollution due to the use of pesticides and herbicides is a 20 common threat found in waterways throughout the world. As the use of these chemicals continue, their toxicity and impact on both the environment and humans is under constant scrutiny with constantly lowering maximum contaminant level (MCL) and maximum residual levels (MRL) set by the Environmental 25 Protection Agency (EPA). In order to fully appreciate the scope and impact of pesticide and herbicide pollution, in-situ detection techniques need to be developed to more accurately pinpoint the sources and broader impact that these pollutants have on the overall environment. Techniques such as ultra and high 30 performance liquid chromatography (UPLC), gas chromatograph (GC) and enzyme-linked immunosorbent assays (ELISA) are commonly used for the detection of pesticides and herbicides in drinking water 1-4. Although these techniques are very sensitive with detection limits below various MRL and MCL levels, the 35 inability for *in-situ* analysis, long processing times, the requirement of various extraction techniques and an extensive amount of necessary equipment limit the flexibility of detecting pesticides and herbicides in real-time format as well as in remote locations. Therefore, there is an urgent need to develop novel 40 analytical systems capable of highly sensitive, selective, real time detection of pollutants in drinking and surface water. Surface enhanced Raman scattering (SERS) is an analytical technique that enhances traditional Raman scattering to allow detection of molecules at ultra low concentrations. It was 45 eventually determined that localized surface plasmon resonance

(LSPR) of noble metal substrates was the major determining factor in the enhancement of the Raman signal^{5, 6}. With a better understanding of how SERS enhancement works, recent research has focused on the creation of suitable SERS substrates using 50 various techniques and methods⁷. However, as the technology advances, a focus towards the creation of SERS systems that can actively detect target molecules in real time is necessary. By combining the high sensitivity of SERS and the mobility and ease of use of microfluidic devices, a complete system for the in-situ 55 detection of targets of interests can be created. For example, continuous in-situ SERS sensors have been created that take the advantages of microfludic channels using colloidial and droplet techniques⁸⁻¹⁰, and various deposition and etching techniques¹¹⁻¹³. These systems are capable of excellent SERS enhancement, 60 however they can be handicapped by additional bonding steps, advanced fabrication techniques such as E-beam, and the necessity for constant replenishing of nanoparticles and additional fluids. To fully optimize the SERS microfluidic device and ensure full integration of the SERS substrate and the 65 microfluidic system, fabrication of the SERS substrate can be performed within the microfluidic itself^{14, 15}, allowing for easy integration and immediate application.

There has been recent publications displaying the production of SERS substrates¹⁶ and the fabrication of microfluidic integrated SERS devices^{14, 17} using galvanic replacement reactions. The use of galvanic replacement allows for the creation of a cheap, easy to fabricate, efficient and highly sensitive SERS substrate. However, little work has been performed on controlling the size, shape and density of the particle created using galvanic replacement. In this article we present a facile, *in-situ* and easily

reproducible method for the microfluidic fabrication of silver nanoparticles (AgNPs) based active SERS substrate for SERS detection by galvanic replacement of pre-patterned copper (Cu) in microfluidic channel. By using the advantages of microfluidics 5 we are able to control the size and density of AgNPs, while still taking advantage of an ease to perform technique such as galvanic replacement. Another advantage of this technique is the ability to control the shape and size of the SERS detection area through pre-patterned Cu substrate, allowing for precise control 10 of location, high reproducibility and consistent results. Crystal violet is first used as a model compound to demonstrate the effectiveness of the as-prepared microfluidic-SERS sensing system. Its further application for sensitive detection of pesticide and herbicide such as Carbofuran and Alachlor was also 15 demonstrated. This study opens a new avenue to fabricate an integrated microfluidic-SERS sensing system with high performance.

Experimental

Chemicals and reagents

20 Silver nitrate (99.85%, Acros) was used as metal precursor for insitu synthesis of silver nanoparticles within a microfluidic channel through galvanic replacement. Silver nitrate solutions were dissolved in Ethylene Glycol (EG, Sigma Aldrich). Crystal violet (CV, Sigma-Aldrich) was applied as the model compound 25 to characterize the effectiveness of the as-developed in-channel SERS system, and Carbofuran and Alachlor (Sigma-Aldrich) were used as the target pesticide and herbicide for a demonstration of real world applications. All SERS solutions were prepared with deionized water (18.2 M Ω cm) from a 30 Barnstead DI water system.

Fabrication of microfluidic device with pre-patterned Cu substrate

In order to conduct in-situ galvanic replacement of Cu within the microfluidic channels, the Cu substrates should be integrated into 35 the microfluidic channel. Therefore, Cu substrates were prepatterned on Si substrate using standard photolithography and lift-off techniques. Briefly, a 100 nm thick SiO₂ insulating layer was first grown on Si wafers and a 300 nm layer of lift-off resist was spin-coated on the wafer followed by a 300 nm layer of 40 photo resist. Exposure was performed on a Karl Suss MJB4 Mask Aligner using the appropriate mask. After developing in MICROPOSITTM MFTM CD-26 Developer, Cr (10 nm) and Cu (100 nm) were sequentially deposited on the wafer in an E-beam evaporator. Finally, the lift-off procedure was performed to 45 generate the Cu susbtarte on the substrate. Meanwhile, standard soft lithography techniques were applied to create the polydimethylsiloxane (PDMS) microfluidic channels. Briefly, SU-8 2025 negative resist (Microchem) were spin-coated on 4" silicon wafers. Exposure with the mask and development with 50 propylene glycol methyl ether acetate (PGMEA) produced channels with width of 100 µm and height of 25 µm. PDMS (Sylgard 184, Dow Corning) was mixed at a 10:1 ratio and poured over the SU-8 mold which was then baked at 80 °C for 1.5 hr to create the final channel. To complete the device 55 fabrication the PDMS channel was plasma bonded to the Si substrate containing the pre-patterned Cu substrates and then assembled with appropriate connectors to form a microfluidic

In-situ preparation of silver nanoparticles as a SERS-active 60 substrate

For *in-situ* preparation of highly active SERS substrate within a microfluidic channel, a solution of 9 mM AgNO3 in EG was pumped through the microfluidic channel at a flow rate of 5 μL/min for 5 s for the galvanic replacement of pre-patterned Cu 65 with Ag⁺. DI H₂O is then pumped through the channel to rinse any excess EG and AgNO₃ and to stop the replacement reaction. After the replacement reaction a dense layer of Ag nanoparticles (AgNPs) with a diameter in the range of ~50 nm-100 nm decorated on the Cu substrate surface. The replacement reaction 70 created a highly dense Ag nanoparticle substrate for in-channel SERS experiments. The advantages of using the microfluidic device and pre-patterned Cu substrate are clearly evident, as the optimized structures are made quickly using very low reagent concentrations at specific locations and the microfluidic channel 75 allows for the immediate use of the substrate for subsequent SERS experiments. The effects of operating conditions such as AgNO₃ concentration, flow rate, reaction time, and temperature on the morphology of nanostructures were also systematically investigated and discussed in subsequent section.

80 Characterization and SERS equipment

Field emission scanning electron microscopy (FE-SEM) was conducted on a JEOL 6335F FESEM (10 kV operating voltage) equipped with a Thermo Noran EDS detector. Raman experiments were conducted using a Reinshaw 2000 Ramascope 85 Micro-Raman equipped with a 514 nm argon-ion laser (50 mW) for crystal violet experiments and 633 nm (50 mW) for Carbofuran and Alachlor experiments, respectively. For a typical SERS measurement, a 20× Leica microscope long objective lens was used to focus the laser beam onto the sample on the SERS 90 substrate for in-channel detection of crystal violet, Carbofuran and Alachlor due to the thickness of PDMS microfluidic channel.

Results and Discussion

In-channel Silver Galvanic Replacement of Copper Substrate

Implementing a microfluidic channel for the galvanic 95 replacement of Cu substrates allowed for the customization, localization and optimization of AgNPs not previously investigated in SERS substrate fabrication using galvanic replacement. Previous implementations of this technique generally involve the immersion of a particular substrate (Cu, Al) 100 into an AgNO₃ solutions of varying concentration 16, 18-20, which generally produces a single structure with little ability for customization and flexibility in more advanced SERS experiments. As shown in Figure 1a, this familiar Ag structure is easily reproduced within the microfluidic channel using the in-105 situ replacement technique. However, because of the small diffusion distances and constant replenishment of AgNO3 to the Cu surface, the Ag nanostructured substrate is fabricated in as quickly as 5 s with 9 mM AgNO₃ solution. Initial experiments

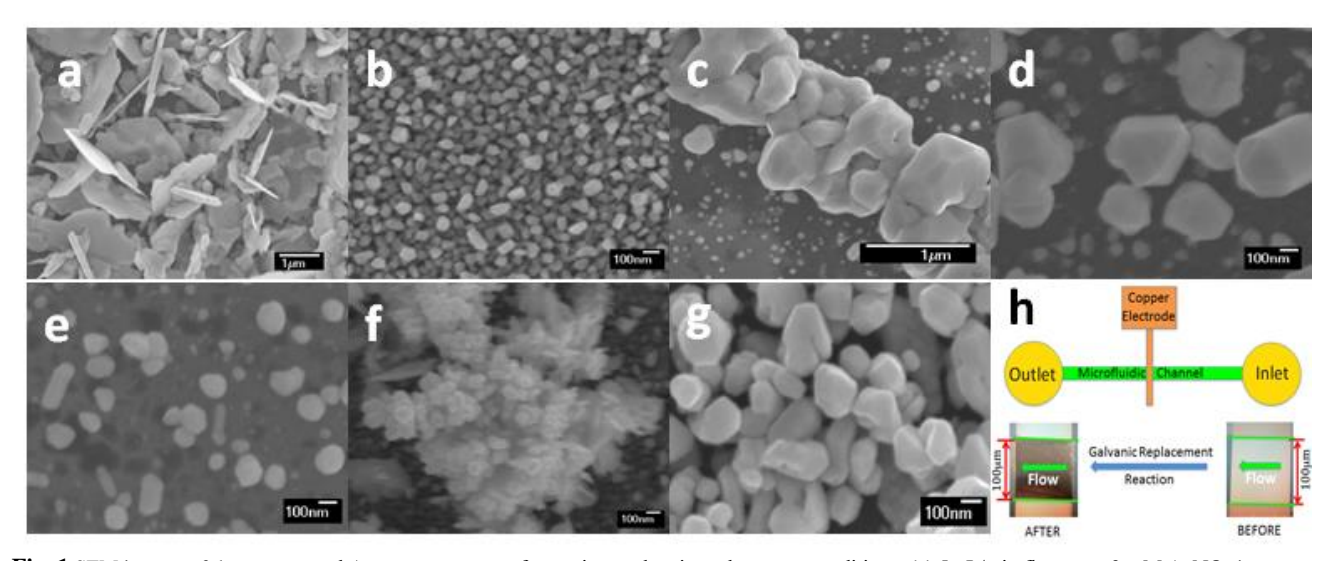


Fig. 1 SEM images of the as-prepared Ag nanostructures after various galvanic replacement conditions: (a) 5 μL/min flow rate, 9 mM AgNO₃ in water, room temperature for 5 s; (b) 5 μL/min flow rate, 9 mM AgNO₃ in EG, 100 °C for 5 s; (c) 5 μL/min flow rate, 9 mM AgNO₃ in EG, room temperature for 3 minutes; (d) 5 µL/min flow rate, 9 mM AgNO₃ in EG, 180 °C for 5 s; (e) 5 µL/min flow rate, 4.5 mM AgNO₃ in EG, 100 °C for 5 s; (f) 5 µL/min flow s rate, 18 mM AgNO3 in EG, 100 °C for 5 s; (g) 5 µL/min flow rate, 9 mM AgNO3 in EG, 100 °C for 30s, and (e) Schematic of the experiment set-up and the optical images of the patterned Cu structure before and after galvanic replacement with Ag under the optimal replacement conditions in (b).

were run to narrow down the concentration range of AgNO₃ solution and reaction time. It was found that shorter running times at higher AgNO3 concentrations created a denser layer of 10 AgNPs. Growth directing agents such as polyvinylpyrrolidone (PVP) and hexadecyltrimethylammonium bromide (CTAB) were also investigated, however because of the short reaction time little to no effect was seen on the formation of Ag nanoparticles, and the use of these reagents generally require organic solvents to 15 fully clean the AgNPs to remove their residues. Unlike other studies, this research shows that by changing the solvent used and other minimal adjustments to operating conditions, the size, shape and density of the Ag nanostructures can be controlled.

The effects of operating conditions on silver nanostructure 20 growth

Unlike previous work implementing bulk galvanic replacement for the fabrication of SERS nanostructures, the shape and density of the Ag nnaostructures in microfluidic channel were controlled in order to maximize the SERS intensity. The effects of operating 25 conditions such as AgNO₃ concentration, temperature and reaction time on the morphology of Ag nanostructures were first investigated. Initial experiments were conducted using water as the solvent, however, it was quickly discovered that individual parameters had little effect on the growth of the Ag 30 nanostructures and the size and density could not be controlled. In place of water, EG was used as the solvent in a role similarly used in the polyol process for the fabrication of silver nanostructures in solution 21, 22, in which EG acts as both a solvent and reducing agent allowing for the growth of silver 35 nanostructures on prefabricated seeds. However, the traditional polyol process creating AgNPs in solution may take several hours and requires several steps to fabricate and recover the final AgNP product²³. Also, without any firm substrate or recovery process, the Ag nanoparticles have a limited use as a SERS material. On 40 the contrary, by combining EG with the galvanic replacement reaction in this study, some control over the size, shape and density of Ag nanostructures in microfluidic channel can be achieved in a much quicker and efficient manner, allowing for the

creation of a SERS substrate with a much wider range of 45 application.

Figure 1b-g shows a series of SEM images from experiments run using EG as a solvent for the galvanic replacement reaction. Each experiment displays a change in one of the variables of the experiment in order to understand how it affected the overall 50 replacement reaction between Cu and Ag⁺. Figure 1b presents a typical SEM image of the final SERS substrate prepared under the optimum conditions, which was used for subsequent SERS experiments. The optimum conditions used for the results in Figure 1b were 5 µL/min flow rate of a solution consisting of 9 55 mM AgNO₃ in EG. The experiment was run at 100 °C for 5 s on 100 nm thick pre-patterned Cu substrate. One can see from Figure 1b that a dense layer of AgNPs ranging in size from 50-100 nm was specifically fabricated on pre-patterned Cu substrate while there is no Ag formed in other area in the microfluidic 60 channel. The advantage of this SERS substrate over the previously reported SERS substrates fabricated using galvanic replacement is the creation of multiple AgNPs which are multifaceted with an increased number of sharp edges and corners, suitable for SERS experiments. In addition, the smaller 65 Ag nanoparticle size obtained could create a SERS substrate with a much larger surface area containing many more "hotspots" which are favorable for SERS detection. Fig. 1f presents schematic of the experiment set-up and the optical images of the patterned Cu structure before and after galvanic replacement with 70 Ag under the optimal replacement.

The remaining images shown in Figure 1a-g demonstrate the effect each parameter has on the overall SERS substrate and the ability to have some control of Ag nanostructures over the replacement reaction. Figure 1c shows that a long Ag nanocable 75 can be generated using 9 mM AgNO₃ in EG at room temperature for 3 minutes. At room temperature the Arrhenius equation tells us the reaction rate of the AgNO3 with the Cu substrate is much lower than that at 100 °C replacement reaction. This causes little to no reaction to happen at short time frames such as the 5 s used

for previous experiments. The lower reaction and diffusion rates also create less seeding points on the Cu layer, creating the less dense AgNP areas around Ag nanocable. Because of this lower seeding area, as the AgNO3 is continuously pumped through the 5 microfluidic channel, Ag growth preferably takes place along the previously replaced substrate instead of creating new seeded areas along the Cu substrate, thus creating large Ag structures

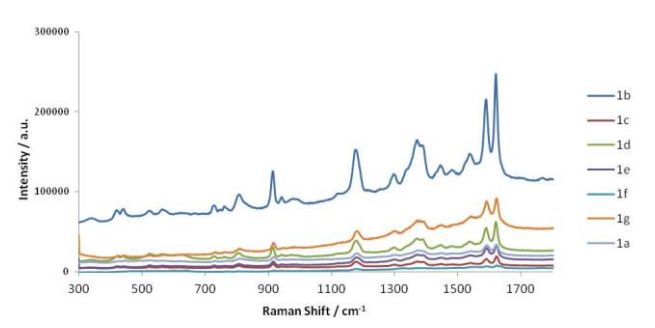


Fig. 2 SERS spectra for 500 nM crystal violet on various SERS substrates 10 depicted in Figure 1.

instead of the densely populated AgNPs SERS substrate as obtained in Figure 1b. The effect of a higher temperature was also investigated as shown in Figure 1d. This experiment was run for 5 s similar to experiment for Figure 1b and with a solution of 15 9 mM AgNO₃ in EG at 180 °C. As seen in the SEM image, the size of the AgNPs are much larger and less dense than that obtained in Figure 1b. When this experiment was allowed to continue for a longer period of time, similar morphology to Figure 1c would be observed as the AgNPs would fuse and form 20 larger structures with large void space surrounding them. Figure 1c and 1d indicated that once the Ag seed forms on the Cu substrate, further Ag growth preferably happens at these seeds, preventing the formation of well-distributed dense AgNP structures required for highly active SERS substrates. By setting 25 our experimental temperate at 100 °C, we balance the reaction and diffusion rate of AgNO3 at the Cu surface, allowing a large number of seeds to be developed, thus creating a much denser AgNP substrate.

The effect of AgNO₃ concentration on the replacement process 30 was also investigated. The concentration of AgNO₃ used in these experiments is much lower compared to previous bulk galvanic replacement studies and the AgNO3 concentration plays a large role in creating the optimal SERS structure for sensing. Figures 1e and 1f display the results from experiments which run for 5 s 35 at 100 °C using 4.5 mM and 18 mM AgNO₃ respectively. As shown in Figure 1e, the lower AgNO₃ concentration creates fewer seeding points and thus results in a sparse layer of AgNPs even though the AgNO3 concentration used here is only half that of experiment in Figure 1b. In addition, the AgNPs are larger in 40 diameter obtained in Figure 1e than in Figure 1b because of the growth along a few spots instead of evenly across the surface. Increasing the AgNO₃ concentration to 18 mM did create a denser AgNPs layer similar to that in Figure 1b, however the excessive amount of Ag+ in solution caused the Ag structures to 45 grow into large vertical structures. Unlike a monolayer of AgNPs (Figure 1b) that would be suitable for SERS experiments, these larger Ag structures (Figure 1f) would make it difficult to create reproducible SERS data. In Figure 1g the effect of increased

reaction time are demonstrated. With the increase of reaction time 50 from 5 s to 30 s, a thick layer of AgNPs are created, however the size of the particles are much larger than that observed in Figure 1b. The size increase of AgNPs decreases the number of available "hotspots", therefore potentially decreasing the overall efficiency of the substrate to act as a SERS surface.

55 In-Channel SERS Sensing

To demonstrate the performance of the galvanic replaced SERS substrate, experiments were carried out using crystal violet as a model compound on all substrates prepared in Figure 1. A 514 nm Ar-ion laser was used to measure the Raman spectra using a 60 20× objective lens and the acquisition time was set for 10 s for each experiment. The experiments were first performed on the SERS substrate by removing the microfluidic channel in order to identify the best SERS substrate resulted from optimized replacement reaction conditions for future in-channel SERS. In 65 each experiment 1 µL of 500 nM crystal violet was placed on the SERS substrate and measurements were immediately taken.

Figure 2 displays the Raman spectra for all 7 experiments demonstrated in Figure 1 and are labeled corresponding to the individual SEM images in Figure 1. As seen from Figure 2 the 70 optimized structure from Figure 1b clearly provides the strongest SERS signal, with the characteristic CV bands at the wave numbers of 1620, 1588, and 1388 cm⁻¹, which correspond to ring C-C stretching and N-phenyl stretching within the CV structure, clearly visible. The rest of the Raman spectra show visible CV 75 peaks with the denser structures of Figures 1d and 1g providing slightly higher intensity than those substrates with lower AgNPs density. The relatively lower SERS intensity generated from substrates of Figures 1c and 1f can be attributed to the large void space between the Ag structures on the substrate, resulting in 80 lower enhancement of Raman signal. The performance comparison of the different Ag substrates allows us to better understand the importance of surface morphology and the total number of hotspots available for SERS, thus determining the optimized galvanic replacement reaction. Whereas it has been 85 shown that single hotspot and single molecule detection can lead to high enhancement factors for Ag SERS substrates, 6, 24 it is important to realize that the overall enhancement of the Raman signal from the substrate is largely dependent on the amount of target analyte adsorbed on the surface under the laser beam spot. 90 Creating SERS substrates that can maximize the amount of molecules that adsorb to the SERS substrate surface under laser beam spot is important in generating reliable SERS devices.

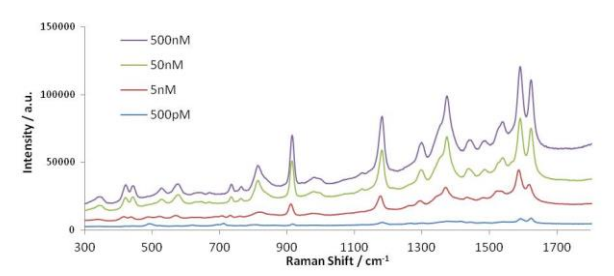


Fig. 3 In-channel SERS spectra of crystal violet on the SERS substrate in 95 Figure 1b after being pumped through the microfluidic device for 20 min.

To further demonstrate the advantage of the microfluidic SERS substrate, in-channel experiments were run on the best

SERS substrate (Figure 1b) using crystal violet as a model compound. Due to the thickness of PDMS channel, a 20× far focus objective lens was used to allow the device to fit within the Raman system. In this experiment the in-situ replacement of the 5 Cu substrate and in-channel SERS detection took place without the removal of the microfluidic channel, allowing for rapid fabrication and detection of the target analyte. The in-channel SERS detection was conducted by pumping the CV solution (500) pM, 5 nM, 50 nM, 500 nM) through the microfluidic channel at a 10 flow rate of 5 µL/min for 20 min. As shown in Figure 3, a 500 pM CV solution can easily be detected and the SERS signal shows concentration-dependent behavior as the Raman intensity increases with increasing CV concentration.

In order to quantify the SERS amplification of the as-prepared 15 microfluidic-SERS sensing system, the enhancement factor (EF) was calculated according to the in-channel experimental results. The most accepted method of calculating the enhancement factor of a SERS substrate is using the following equation²⁵:

$$EF_{app} = \frac{I_{SERS} / N_{SERS}}{I_{NR} / N_{NR}}$$
 (1)

20 Where I_{SERS} is the intensity of the SERS signal; N_{SERS} is the number of molecules contributing to I_{SERS} ; I_{NR} is the intensity of the Raman signal at the same frequency on a silicon substrate; N_{NR} is the number of molecules of the target species contributing to I_{NR} . However, because of the nature of the in-channel SERS 25 experiments, it is difficult to estimate the number of molecules absorbed on the substrate surface. Therefore, in order to estimate the enhancement factor of the substrate an apparent enhancement factor (EF_{ann}) is used instead to correlate with the concentration of analytes. Therefore the equation used to calculate the 30 enhancement factor is as follows:

$$EF_{app} = \frac{I_{SERS} / C_{SERS}}{I_{NR} / C_{NR}}$$
 (2)

Where I_{SERS} and I_{NR} share the same definition as those in Equation 1, and C_{SERS} and C_{NR} are the concentration of molecules contributing to I_{SERS} and I_{NR} , respectively. Using this equation 35 gives a better understanding of the actual enhancement capable of the microfluidic-SERS system as it reaches equilibrium. Thus, the calculated EF_{app} of the microfluidic system is ~2.2 ×10⁷, which is sufficiently high to detect single molecules²⁵.

Surface Regeneration

40 One aspect of SERS and SERS substrates is the additive effect of molecules as they adsorb to the substrate surface. Chemisorption of these molecules make it difficult for real-time analysis as all Raman active molecules adsorbed on the substrate contribute to the overall SERS spectra. The ability to wash and reuse the 45 microfluidic-SERS substrate while it is still in the microfluidic channel is an important attribute and necessary if the device is to perform as a real world pesticide detection system.

The degradation of molecules by UV-light is a well researched topic and has proven effective with molecules such as crystal 50 violet^{26, 27}. To test the ability of UV-light to remove crystal violet

from the SERS substrate in microfluidic channel, test samples were created by flowing 500 nM crystal violet solutions through the fabricated SERS device for 20 minutes. Initial experiments used a 365 nm UV-lamp placed over the microfluidic SERS 55 device while DI H₂O was pumped through the microfluidic channel at 5 µL/min for 10 minutes. Figure 4 displays the UV only cleaning results. SERS spectra post cleaning still display some minor peaks although the peaks are slightly different than traditional crystal violets peaks. The remaining peaks may 60 demonstrate the degradation of crystal violet molecules; however there is still adsorption of the intermediate products on the substrate surface and theses molecules are still Raman active.

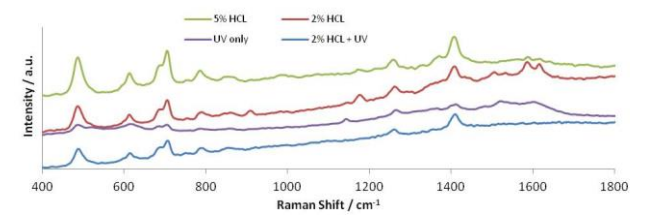


Fig. 4 Comparison of SERS substrate regeneration techniques

Another method for the removal of organics is demonstrated by the use of HCl to recover crystal violet in dye removal processes²⁸. This method was also tested and the results are demonstrated in Figure 4. In the experiment 2% and 5% HCl solutions are pumped through the microfluidic device for 10 70 minutes at 5 μL/min. The results display that an increased amount of CV was removed at higher HCl concentrations, however, it was observed the damage of the SERS substrate occurred at 5% HCl concentration. Since both methods showed promise in removal of crystal violet the final experiment used a 2% HCl 75 solution combined with 365 nm UV-light. The solution was pumped through the microfluidic device at 5 µL/min for 10 minutes under UV light. The results are displayed in Figure 4 and show the only peaks remaining are those of PDMS. All crystal violet and intermediate product SERS spectra are removed 80 and a pristine SERS substrate is created. The benefits of this system are the small footprint of the UV-light and the low amount of HCl solution used which allows for the easy integration of the regeneration system with the overall SERS device.

85 Adsorption Kinetics

Understanding how crystal violet adsorbs to the SERS substrate will yield valuable information when running experiments for later pesticide detection. Data collected from microfluidic-SERS experiments was fitted to both the Langmuir and Freundlich 90 adsorption isotherms. Since the amount of adsorbed species on the surface of the substrate is extremely small and difficult to measure, the intensity of the SERS signal is used as a representation instead. This provides a simple solution in attempting to model adsorption of molecules on the SERS 95 substrate, however the enhancement factor and therefore intensity of the Raman signal is greatly reliant on the location of the adsorbed species on the substrate. Molecules located close to or in hotspots on the substrate surface contribute much more to the overall EF than the majority of molecules. Studies between 100 molecule location and EF have shown that the average

enhancement can be as much as 300 times smaller than the maximum EF and that 80% of the SERS signal is contributed by 0.64% of the molecules situated close to or in hotspots²⁹. Therefore, allowing the sample collection to run until it reaches 5 equilibrium creates much more consistency in the SERS average intensity collected and thus provides a better understanding of adsorption and application of the isotherms.

The Langmuir equation can be used to describe a single molecular layer of adsorbents on the SERS surface. The traditional Langmuir equation can be rearranged into a linear form and modified as shown below,

$$\frac{C_e}{I} = \frac{1}{K_L q_m} + \frac{1}{q_m} C_e \tag{3}$$

where I is the measured intensity of the 1177 cm⁻¹ crystal violet peak at equilibrium, C_e is the liquid-phase concentration of crystal violet, K_L is a measurement of the intensity of sorption, and q_m is the area occupied by a monolayer of adsorbent, or the maximum adsorption capacity of the substrate. The 1177 cm⁻¹ peak intensities were measured from the four Raman spectrums in Figure 3. When graphing C_e /I vs. C_e , q_m and K_L can be determined from the slope and intercept of the line displayed in Figure 5. The R^2 value for the graph of .9997 signifies a good fit of the data, and q_m and K_L are determined from the slope and intercept and plugged into the original equation. Another characteristic of the Langmuir isotherm can be determined from the displayed in Figure 6.

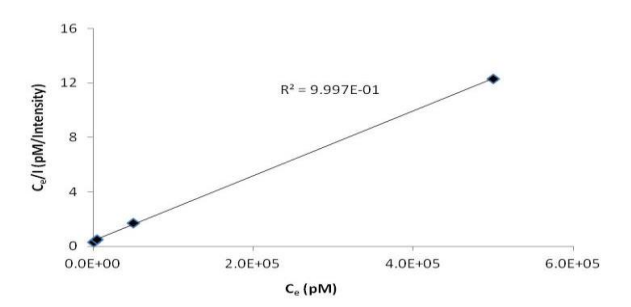


Fig.5 Linear graph of Langmuir equation for crystal violet intensities

R_L values between 0 and 1 indicate favorable adsorption of the crystal violet on the substrate surface, while higher R_L values at lower concentrations display the crystal violet adsorption is more favorable at lower concentrations. However, this data is based off intensity and not concentration of adsorbed species and a different set of information can be inferred from the graph. As mentioned above SERS substrates have a limited amount of hot spots that contribute the most to the overall EF and intensity. Figure 6 infers that at lower concentrations the majority of the intensity is from a small number of molecules adsorbed at or near the hotspots. As concentration increases the overall EF contribution of the hotspots is diminished, displaying a less favorable adsorption as depicted in Figure 6.

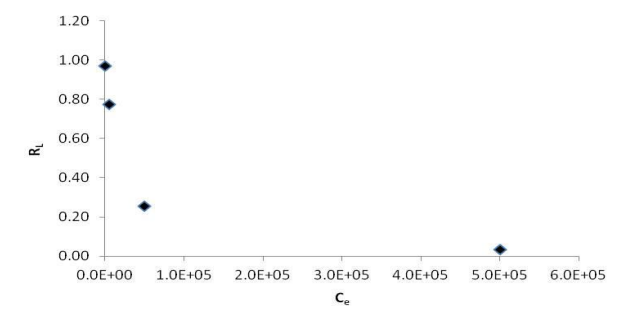


Fig. 6 Separation factor at various crystal violet concentrations (pM)

The Freundlich isotherm differs from the Langmuir in that it does not restrict the amount of adsorbent to a single monolayer on the substrate surface. The Freundlich isotherm has been traditionally used for more heterogeneous surfaces^{30, 31}, and comparison to the Langmuir isotherms will help in determining the type of adsorption on the SERS surface. The most common form of the Freundlich equation is below;

$$I = K_F C_e^{1/n} \tag{4}$$

Where K_F is a constant related to the bonding energy of adsorbents and 1/n is a measure of the surface heterogeneity. Plotting $\ln I$ vs. $\ln C_e$ gives an intercept of K_F and a slope of 1/n and is displayed in Figure 7. The R^2 value of 0.9103 indicates that the system is more favorable towards single mono-layer Langmuir adsorption; however, the heterogeneous nature of the galvanic replaced Ag nanoparticles leads one to expect the substrate to also display some adsorption characteristics of the 60 Freundlich adsorption.

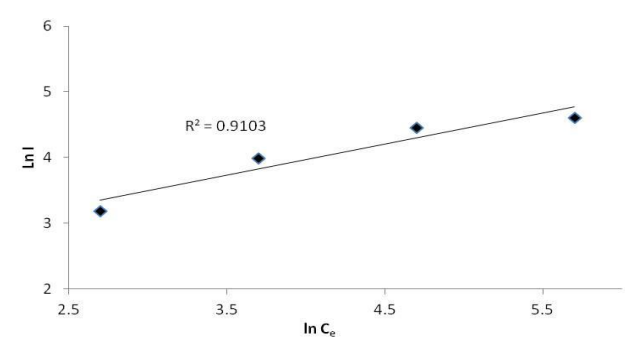


Fig. 7 Freundlich plot of crystal violet intensities

Figure 8 is a comparison of the experimental, Langmuir and Freundlich data. One can see that the Langmuir isotherm shows a favourable fit to the experimental data and will work well to predict unknown concentrations based on given intensities. The Freundlich curve shows some fit at lower concentrations, however as concentration increases the expectancy for increased adsorption of molecules and therefore increased intensity is not in good agreement with experimental data.

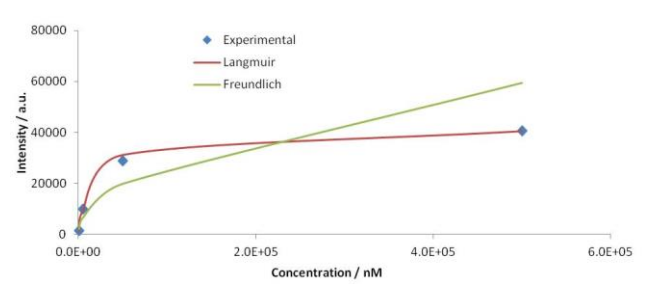


Fig. 8 Comparison of experimental, Langmuir and Freundlich data.

Microfluidic-SERS detection of pesticides

The ability for real-time detection of pesticides is an important 5 challenge with no real solutions. Carbofuran is a highly toxic carbamate pesticide, currently banned in the European Union (EU) but is still used throughout the world, and is only now facing a ban in the US after a voluntary stoppage of use³². Carbofuran is a neurotoxic poison, endocrine disruptor and 10 reproductive intoxicant that is known to be fatal to humans and wildlife. Meanwhile, Alachlor is a widely used herbicide banned in the EU but still sees broad use in the United States. Although the herbicide is only classified as slight toxic by the Environmental Protection Agency (EPA), long term effects of the 15 compound such as liver, kidney, spleen damage and cancer have caused concern over its widespread use³³. Therefore, to evaluate the sensing performance of the as-developed microfluidic-SERS system in pesticide and herbicide detection, Carbonfuran and Alachlor were selected as model compounds.

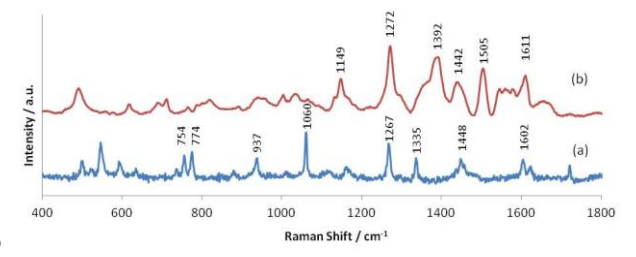


Fig. 9 Comparison of (a) Raman spectra of solid Carbofuran and (b) SERS spectra of 500 nM aqueous Carbofuran.

Pesticide detection experiments were performed following a procedure similar to in-channel CV experiments described before. 25 Briefly, the pesticide is pumped through the microfluidic device at 5 µL/min for 20 minutes, after which SERS experiments are conducted. Figure 9 shows the SERS spectrum of 500 nM Carbofuran and Raman spectrum of the solid Carbofuran. Changes in Raman shift and peak shape can help determine what 30 interactions the molecule is having with the SERS surface. A shift and change of the doublet benzene ring C=C stretch from 1624 cm⁻¹ (typical) to 1611 cm⁻¹ indicate some interaction between the benzene ring and the Ag surface. Strong peaks located at 1505 cm⁻¹ and 1392 cm⁻¹ may also indicate interactions 35 between the furan group and Ag surface. There is no apparent shift observed for the C-H benzene bending band (1267 cm⁻¹ vs. 1272 cm⁻¹) and the bending band of CH₃ groups attached to the furan molecule (1448 cm⁻¹ vs. 1442 cm⁻¹) in both solid Carbofuran Raman spectrum and its SERS spectrum, probably 40 indicating weak interaction at these points with the SERS substrate.

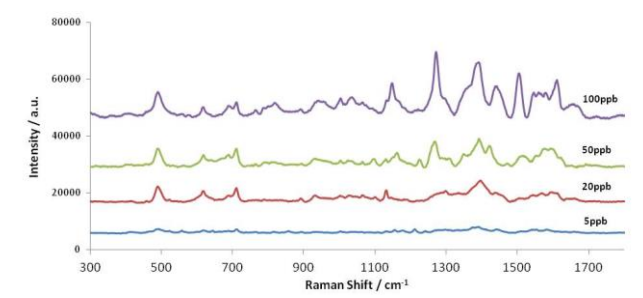


Fig. 10 Normalized SERS spectra of Carbofuran at 5 ppb, 20 ppb, 50 ppb and 100 ppb, respectively.

Figure 10 and 11 display the concentration-dependent SERS signals for Carbofuran and Alachlor, respectively. One can see that both Carbofuran and Alacholor can be easily identified through in-channel SERS analysis and the Raman intensity shows concentration-dependent behavior, indicating that the presence of 50 PDMS does not block the SERS signal of pesticides. Such superior enhancement of in-channel Raman signal and ultrasensitivity to analyte can be ascribed to the synergistic effect of several factors such as large surface area of SERS substrate for adsorption of analytes, and the electromagnetic effect and 55 chemical effect of numerous "hot spots" resulted from closely contacted AgNPs. Concentrations as low as 5 ppb can be detected for both Carbofuran and Alachlor, indicating excellent sensitivity. Combined with the finger-printing spectrum of each compound, these features allow sensitive and selective detection of pesticides 60 and herbicides.

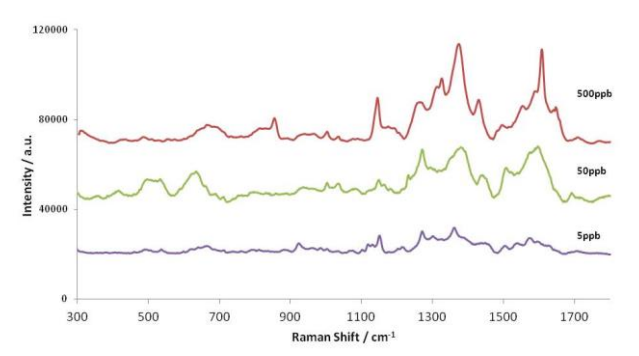


Fig. 11 Normalized SERS spectra of Alachlor at 5 ppb, 50 ppb and 500 ppb, respectively.

Conclusions

fabricated within a microfluidic channel via a facile *in-situ* galvanic replacement reaction method. The as-prepared novel substrate was first evaluated using crystal violate for in-channel SERS detection. An apparent enhancement factor for in-channel of SERS was calculated to be ~2.2 ×10⁷. Its further application for in-channel SERS detection of pesticide and herbicide such as Carbofuran and Alachlor was demonstrated with an excellent limit of detection as low as 5 ppb for both targets. The superior enhancement of in-channel Raman signal and excellent sensitivity to analyte can be attributed to the synergistic effect of several factors such as large available surface of AgNPs for analyte adsorption, and the electromagnetic effect and chemical effect of numerous "hot spots" resulted from closely contacted AgNPs. Compared to other methods, ³⁴ this study provides a

simple and fast method to fabricate *in-situ* active SERS substrate within microfluidic channels and opens a new venue to *in-situ* integration of functional nanostructures within microfluidic devices. The demonstration of sensitive detection of pesticide and 5 herbicide using the combined power of microfluidics and SERS offers a new device to chemical and biological sensing application.

Acknowledgements

This work was supported by the funding from the National Science Foundation. Joseph Parisi also acknowledges the support from NSF GK-12 Fellowship.

Notes

- ^a Department of Chemical and Biomolecular Engineering and
 ^b Department of Biomedical Engineering University of Connecticut, 191
 ¹⁵ Auditorium Road, Unit 3222, Storrs, CT, 06269, USA
 Fax: 1-860-486-2959; Tel: 1-860-486-4554; E-mail:
 ylei@engr.uconn.edu
- † Electronic Supplementary Information (ESI) available: [details of any supplementary information available should be included here]. See DOI: 10.1039/b000000x/

References

- H. Kataoka, H. L. Lord and J. Pawliszyn, Journal of Chromatography A, 2000, 880, 35-62.
 - 2. C. C. Leandro, P. Hancock, R. J. Fussell and B. J. Keely, *Journal of Chromatography A*, 2006, **1103**, 94-101.
- 3. H. Wang, J. Wang, C. Timchalk and Y. H. Lin, *Analytical Chemistry*, 2008, **80**, 8477-8484.
- M. C. Hennion and D. Barcelo, Analytica Chimica Acta, 1998, 362, 3-34
- P. L. Stiles, J. A. Dieringer, N. C. Shah and R. R. Van Duyne, *Annual Review of Analytical Chemistry*, 2008, 1, 601-626.
- 35 6. Y. Fang, N. H. Seong and D. D. Dlott, Science, 2008, 321, 388-392.
- M. J. Banholzer, J. E. Millstone, L. D. Qin and C. A. Mirkin, Chemical Society Reviews, 2008, 37, 885-897.
- H. Chon, C. Lim, S. M. Ha, Y. Ahn, E. K. Lee, S. I. Chang, G. H. Seong and J. Choo, *Analytical Chemistry*, 2010, 82, 5290-5295.
- K. R. Strehle, D. Cialla, P. Rosch, T. Henkel, M. Kohler and J. Popp, Analytical Chemistry, 2007, 79, 1542-1547.
- J. Y. Zhang, J. Do, W. R. Premasiri, L. D. Ziegler and C. M. Klapperich, *Lab on a Chip*, 2010, **10**, 3265-3270.
- 45 11. R. Gordon, D. Sinton, K. L. Kavanagh and A. G. Brolo, Accounts of Chemical Research, 2008, 41, 1049-1057.
 - 12. D. Cialla, U. Hubner, H. Schneidewind, R. Moller and J. Popp, *ChemPhysChem*, 2008, **9**, 758-762.
- B. B. Xu, Z. C. Ma, H. Wang, X. Q. Liu, Y. L. Zhang, X. L. Zhang,
 R. Zhang, H. B. Jiang and H. B. Sun, *Electrophoresis*, 2011,
 32, 3378-3384.
- 14. J. Parisi, L. Su and Y. Lei, Lab on a Chip, 2013, 13, 1501-1508.
- J. Leem, H. W. Kang, S. H. Ko and H. J. Sung, Nanoscale, 2014, 6, 2895-2901.

- 55 16. A. Gutes, C. Carraro and R. Maboudian, Journal of the American Chemical Society, 2010, 132, 1476-+.
 - B. B. Xu, Z. C. Ma, L. Wang, R. Zhang, L. G. Niu, Z. Yang, Y. L. Zhang, W. H. Zheng, B. Zhao, Y. Xu, Q. D. Chen, H. Xia and H. B. Sun, *Lab on a Chip*, 2011, 11, 3347-3351.
- 60 18. Y. G. Sun and G. P. Wiederrecht, Small, 2007, 3, 1964-1975.
- L. Su, W. Z. Jia, D. P. Manuzzi, L. C. Zhang, X. P. Li, Z. Y. Gu and Y. Lei, *Rsc Advances*, 2012, 2, 1439-1443.
- 20. J. F. Betz, Y. Cheng and G. W. Rubloff, Analyst, 2012, 137, 826-828.
- F. Fievet, J. P. Lagier, B. Blin, B. Beaudoin and M. Figlarz, *Solid State Ionics*, 1989, 32-3, 198-205.
- 22. Y. G. Sun and Y. N. Xia, Advanced Materials, 2002, 14, 833-837.
- 23. Y. G. Sun, Y. D. Yin, B. T. Mayers, T. Herricks and Y. N. Xia, *Chemistry of Materials*, 2002, **14**, 4736-4745.
- J. P. Camden, J. A. Dieringer, Y. M. Wang, D. J. Masiello, L. D.
 Marks, G. C. Schatz and R. P. Van Duyne, *Journal of the American Chemical Society*, 2008, 130, 12616-+.
- 25. E. C. Le Ru, E. Blackie, M. Meyer and P. G. Etchegoin, *Journal of Physical Chemistry C*, 2007, **111**, 13794-13803.
- C. Sahoo, A. K. Gupta and A. Pal, Dyes and Pigments, 2005, 66, 189-196.
- F. A. Alshamsi, A. S. Albadwawi, M. A. Alnuaimi, M. A. Rauf and S. S. Ashraf, *Dyes and Pigments*, 2007, 74, 283-287.
- A. Mittal, J. Mittal, A. Malviya, D. Kaur and V. K. Gupta, *Journal of Colloid and Interface Science*, 343, 463-473.
- 80 29. E. C. Le Ru, P. G. Etchegoin and M. Meyer, *Journal of Chemical Physics*, 2006, **125**, 204701.
- G. Annadurai, R. S. Juang and D. J. Lee, *Journal of Hazardous Materials*, 2002, 92, 263-274.
- 31. E. Erdem, N. Karapinar and R. Donat, *Journal of Colloid and*85 Interface Science, 2004, **280**, 309-314.
- E. P. A. U.S, Carbofuran Cancellation Process, http://www.epa.gov/oppsrrd1/reregistration/carbofuran/carbofuran_noic.htm, Accessed August 8th, 2014.
- 33. E.P.A, Basic Information about Alachlor in Drinking Wate, http://water.epa.gov/drink/contaminants/basicinformation/alac hlor.cfms, Accessed August 8th, 2014.
- 34. H.W. Kang, J. Leem and H.J. Sung, RSC Advances, 2015, 5, 51-57.